MATERIALS CHEMISTRY FRONTIERS

CHINESE CHEMICAL SOCIETY

ROYAL SOCIETY OF CHEMISTRY

RESEARCH ARTICLE

View Article Online
View Journal | View Issue

Cite this: *Mater. Chem. Front.*, 2021, **5**, 2261

Full-type photoluminescence from a single organic molecule for multi-signal temperature sensing†

Jing Ma,‡[a] Yusheng Zhou,‡[a] Haiyang Gao,[a] Fangming Zhu[b] and Guodong Liang*[a]

Received 5th January 2021,
Accepted 14th January 2021

DOI: 10.1039/d1qm00023c

rsc.li/frontiers-materials

Photoluminescent materials are one of the most important materials widely used in various fields. They emit normally a single type of photoluminescence at room temperature, either fluorescence (FL), delayed fluorescence (DF), or phosphorescence (RTP). Here, uncommon full-type photoluminescence including concomitant FL, DF, and room-temperature phosphorescence (RTP) from a single organic molecule is reported. The material shows unique aggregation-induced phosphorescence (AIP) and remarkable thermoresponsive persistent phosphorescence (TPP). Interestingly, TPP, together with thermoresponsive FL and DF of the chromophore, gives rise to multiple visual signals including luminescence colour, colour evolution, brightness, and fading rates upon temperature variation, affording a new class of thermoresponsive materials. More importantly, the incorporation of the chromophore into polymers further amplifies its luminescence thermoresponse. In particular, the phosphorescence lifetime of the doped films increases linearly by 8-fold with lowering temperature, which is highly desirable for quantitative temperature sensing but rarely reported. Furthermore, a facile method based on phosphorescence lifetime and image analysis (PLIA) of the doped films is used for quick, visual, and quantitative temperature sensing.

Introduction

Photoluminescent materials are one of the most important materials widely used in various fields including optical devices, displays, biology, information storage, and encryption.[1–13] Photoluminescence (PL) is classified into fluorescence (FL), delayed fluorescence (DF), and phosphorescence, based on how excited molecules return to their ground state. Photoluminescent materials normally emit a single type of photoluminescence at room temperature, either FL, DF, or phosphorescence, depending on their composition, structure, and molecular packing. Compared to short-lived fluorescence, persistent phosphorescence (PP) has attracted increasing attention due to its large Stokes shift and long lifetime.[14–21] However, compared to inorganic counterparts, organic phosphors generally show a relatively short phosphorescence lifetime (<10 ms) at room temperature due to rapid non-radiative decay of triplet excitons.[22–29] To stabilize the triplet excitons, various strategies including crystallization, host–guest inclusion, H-aggregation, and doping in a rigid matrix have been used to achieve efficient RTP in organic materials.[30–33] Although a few classes of organic RTP phosphors have been reported,[34–38] they are very scarce in number compared to fluorescent dyes. Organic RTP chromophores with concomitant FL and DF, are even more rarely documented in the literature.[39]

Thermoresponsive photoluminescent (TRP) materials present a kind of promising functional material with interesting temperature-dependent photoluminescence (PL) properties.[40] The PL colour and brightness of TRP materials change noticeably as a function of temperature, offering them a wide range of applications in sensing, smart optical devices, and so on.[40–43] The thermoresponse of organic fluorescent compounds is mainly based on their thermal transitions such as melting,[44] crystallization,[45] crystal transition,[46,47] and glass transition as temperature fluctuates. The packing and mobility of the fluorescent organic molecules change during the transitions, resulting in obvious TRP properties. Alternatively, labelling organic fluorescent chromophores into thermoresponsive polymers is also used to generate TRP polymers.[48,49] However, TRP materials based on thermal transitions suffer from some inherent limits

[a] *PCFM Lab, School of Materials Science and Engineering, Sun Yat-sen University, Guangzhou 510275, P. R. China. E-mail: lgdong@mail.sysu.edu.cn*
[b] *PCFM Lab, School of Chemistry, Sun Yat-sen University, Guangzhou 510275 P. R. China*

† Electronic supplementary information (ESI) available: XRD spectra, fluorescence microscopy images, scanning electron microscopy images, and temperature sensing based on TBBU crystal films. See DOI: 10.1039/d1qm00023c

‡ These authors contributed equally to this work.

including slow response, a non-linear relationship of PL signals against temperature, and a narrow temperature range (typical <20 °C).[50–52] Therefore, the development of TRP materials with a quick and linear response as well as wide temperature windows is highly desirable for academic research and engineering applications.

Phosphorescence of organic compounds is susceptible to temperature because non-radiative decay of triplet excitons is temperature-dependent. Lowering temperature is favourable for stabilization of triplet excitons and consequent phosphorescence through alleviating thermal perturbation and molecular motion. Compared with fluorescence, phosphorescence is more sensitive to temperature fluctuation. Phosphorescence intensity changes remarkably with temperature variation even beyond the temperature range of phase transition. This offers a valuable opportunity for the creation of organic TRP materials. Indeed, a few organic phosphors with temperature-dependent phosphorescence have been reported recently.[30,53] However, a non-linear relationship of phosphorescence intensity with temperature is obtained, which is adverse to their further applications such as in quantitative temperature sensing. Moreover, the phosphorescence intensity of phosphors depends on many factors such as the concentration of the compounds, and size and thickness of the samples, as well as excitation. Thus, complicated calibration protocols must be applied for quantitative applications. Consequently, although several catalogues of phosphors are reported, few of them are used to sense temperature.

Herein, we report uncommon full-type photoluminescence including concomitant FL, DF, and RTP from a single organic molecule (TBBU) (Fig. 1a). Unusual aggregation-induced phosphorescence (AIP) and remarkable thermoresponsive persistent phosphorescence (TPP) have been investigated. In particular, TPP, along with thermoresponsive FL and DF of the chromophore, gives rise to multiple visual signals including luminescence colour, colour evolution, brightness, and fading rates upon temperature variation, affording a new class of thermoresponsive materials, which are completely different from those of the phosphors[30–32] and the TRP compounds reported (Fig. S1 in the ESI†). More interestingly, the incorporation of the chromophore into polymers further promotes its thermoresponse. The phosphorescence lifetime increases linearly by 8-fold with lowering temperature, which enables quantitative temperature sensing. Such linear relationship of phosphorescence signals with temperature is highly desirable for temperature sensing, but is rarely reported in the literature. Most importantly, taking full advantage of AIP and TPP of the chromophore, a method based on phosphorescence lifetime and image analysis (PLIA) is developed for quick and quantitative temperature sensing through multiple visual signals. Given the good reliability

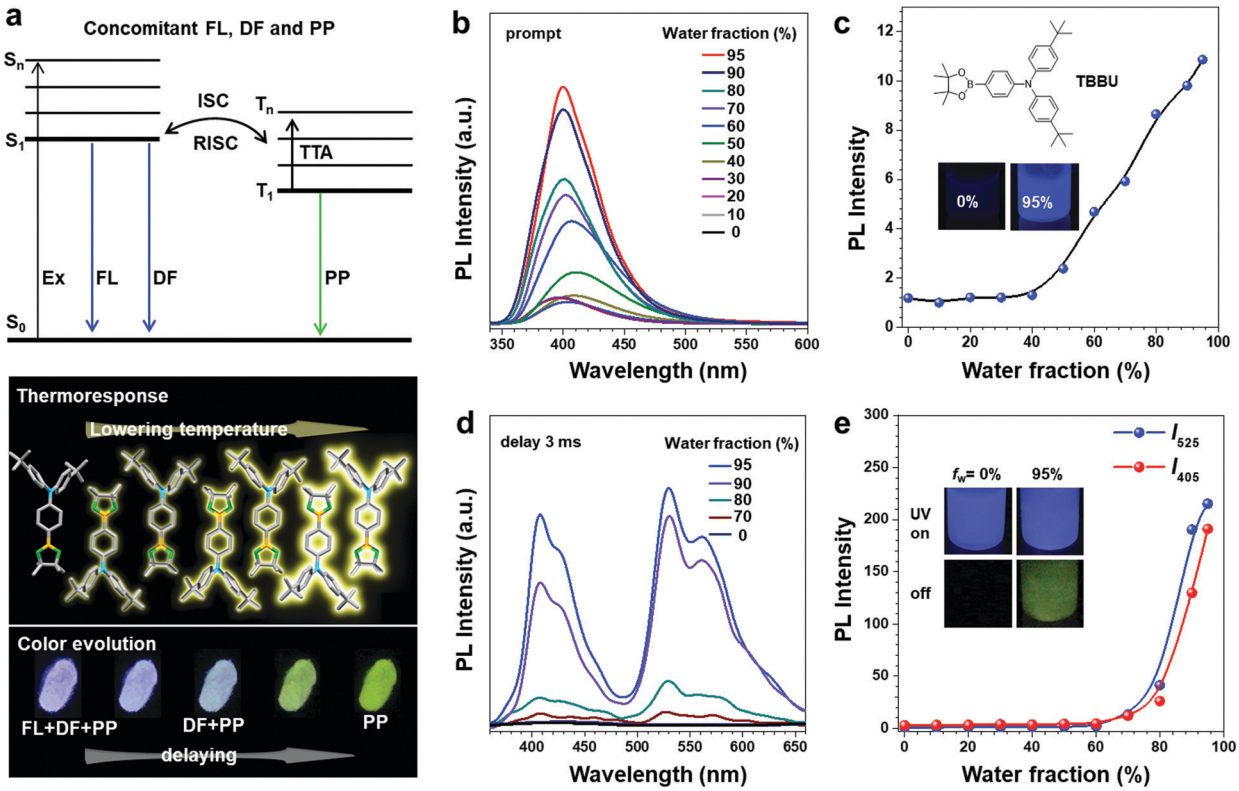

Fig. 1 (a) Schematic illustration of full-type photoluminescence including concomitant fluorescence (FL), delayed fluorescence (DF) and persistent phosphorescence (PP), as well as thermoresponse and colour evolution. (b) Prompt photoluminescence (PL) spectra of the chromophore in THF/H_2O mixtures at various water fractions (0, 10, 20, 30, 40, 50, 60, 70, 80, 90, and 95%). Excitation: 350 nm. (c) PL intensity (at 405 nm) as a function of water fraction. (d) PL spectra (delay 3 ms) of the chromophore in THF/H_2O mixtures at various water fractions (0, 70, 80, 90 and 95%). Excitation: 350 nm. (e) PL intensity (at 405 and 525 nm, respectively) as a function of water fraction.

and accuracy, easy operation, and simple devices, the PLIA offers a new platform for facile temperature sensing.

Results and discussion

Aggregation-induced emission of the chromophore

The chromophore (TBBU) shows good solubility in common organic solvents, such as dichloromethane (DCM) and tetrahydrofuran (THF).[54] DCM solutions of the chromophore (0.1 M) radiate inefficiently under UV (365 nm) lamps. The solutions were cast onto quartz wafers and the solvent was evaporated in air within 30 min to form films. The films emit intense blue light under UV radiation, showing aggregation-induced emission (AIE) characteristics.[55–58] More interestingly, upon switching off the UV lamp, the colour of the films changes from blue into white, and green in turn, and fades quickly, showing RTP characteristics. To further investigate AIE behaviour of the chromophore, photoluminescence (PL) spectra in THF/H_2O mixtures were recorded. Prompt PL at low water fractions ($f_w \leq 40$ vol%) is weak (Fig. 1b and c). With further increasing $f_w \geq 50$ vol%, PL at 405 nm boosts drastically. The PL intensity at f_w = 95 vol% is 10-fold that in pure THF, showing AIE features. Similarly, delayed PL (3 ms) of the chromophore is weak in the mixed solutions at $f_w \leq 50$ vol% (Fig. 1d and e). The delayed PL at 405 and 525 nm increases abruptly with further increasing $f_w \geq 60$ vol%. The PL intensity (405 and 525 nm) at f_w = 95 vol% is 190 and 215-fold that in pure THF, respectively, showing aggregation-induced delayed fluorescence (AIDF) and aggregation-induced phosphorescence (AIP),[54] respectively.

X-Ray diffraction (XRD) spectra are used to investigate the microstructure of the chromophore films and aggregates in THF/H_2O mixtures (f_w = 95 vol%). XRD spectra of both films and aggregates of the chromophore show distinct diffraction peaks (Fig. S2, ESI†), resembling the simulated spectrum from its single crystals. Thus, the chromophore forms crystals during evaporation of the solvent and precipitation in THF/H_2O mixtures. Compared with slow evaporation of solvents (30 min), precipitation of the chromophore in THF/H_2O mixtures (f_w = 95 vol%) takes place much quicker (a few seconds). Such rapid precipitation still leads to crystallization of the chromophore, suggesting strong intermolecular interactions among adjacent molecules. Fluorescence microscopy (FM) and scanning electron microscopy (SEM) were used to observe the morphology of the films and aggregates (Fig. S3, ESI†). Microcrystals with a

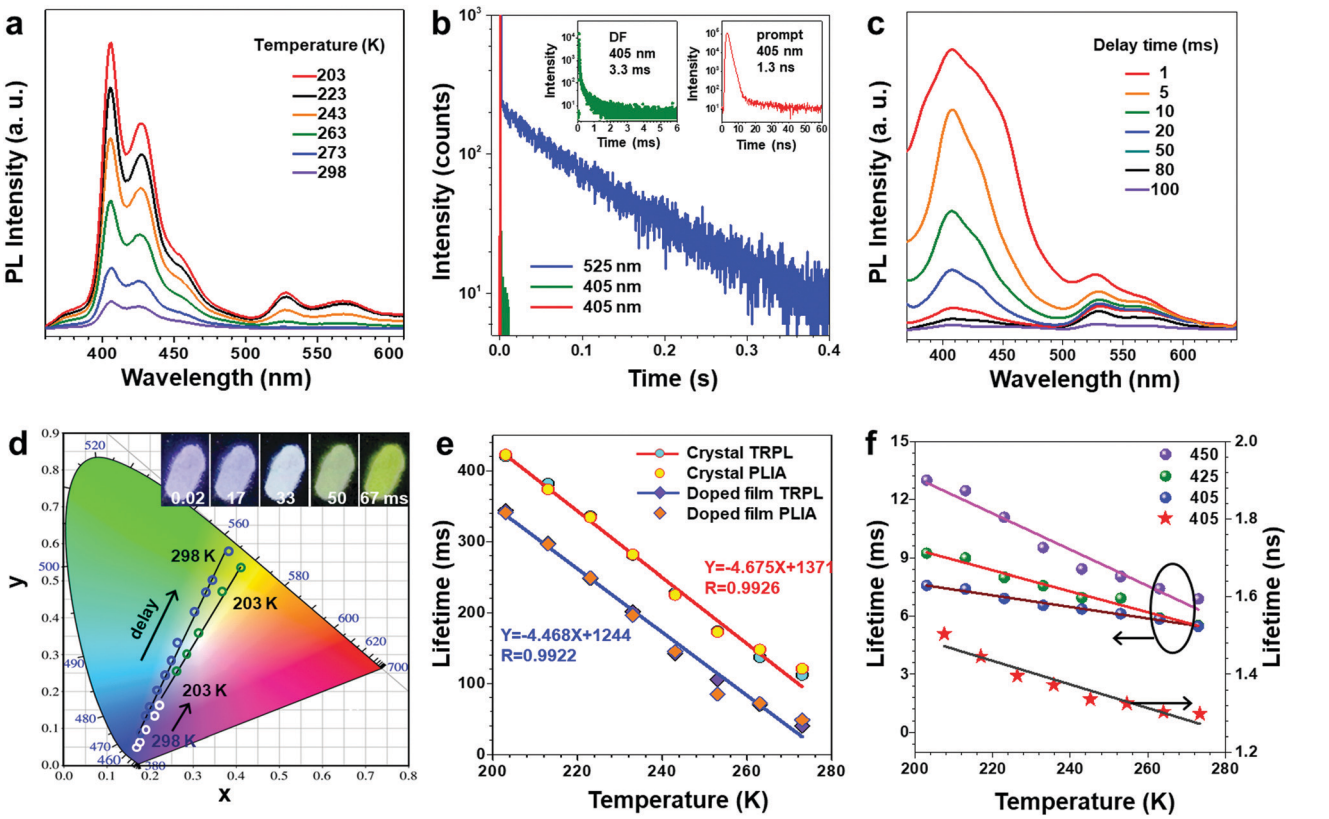

Fig. 2 (a) Prompt PL spectra of the crystal films at various temperatures (298, 273, 263, 243, 223 and 203 K, from bottom to top, respectively). (b) Time-resolved photoluminescence spectra (TPPL) of the crystal films at 525 and 405 nm. (c) PL spectra delayed for various times of the crystal films. (d) The Commission Internationale de l'Eclairage (CIE) coordinates of the PL spectra of the crystal films. The inset shows the digital images of the crystal films (at 203 K) at various delay times (0, 17, 33, 50, 67 ms, from left to right, respectively). (e) The plots of lifetime (at 525 nm) against temperature for the chromophore films and its doped polymer films. (f) The plots of lifetime (at 450, 425 and 405 nm) against temperature for the chromophore crystal films.

diameter of approximately 20 μm are observed for the chromophore films and the aggregates in THF/H_2O mixtures.

Multiple luminescence of the chromophore

The crystal films of the chromophore show multiple luminescence including an intense fluorescence emission in the range of 380–500 nm with a fluorescence efficiency of 64% and a weak phosphorescence emission in the range of 500–650 nm with RTP efficiency of 1.4% at room temperature (Fig. 2a and Fig. S4, S5, ESI†).[54] The fluorescence emission (*e.g.* at 405 nm) contains a short-lived (1.3 ns, fluorescence, FL) and a long-lived (3.3 ms, DF) component. While the phosphorescence emission (*e.g.* at 525 nm) has a long lifetime (*i.e.* 13 ms) (Fig. 2b). After switching off the UV lamp, the crystal emission turns to white and green in turn, and fades quickly. Delayed PL spectra of the crystal films show double emissions peaked at 405 and 525 nm, respectively (Fig. 2c). With increasing decay time from 1 to 100 ms, the PL intensity at 405 nm decreases rapidly relative to the peak at 525 nm due to its short lifetime. The corresponding Commission Internationale de l'Eclairage (CIE) chromaticity coordinates shift linearly from (0.18, 0.09) to (0.39, 0.58), passing through the white region (0.27, 0.33), for the PL spectra delayed from 1 to 100 ms (Fig. 2d). The colour evolution of the chromophore is related to its multiple luminescence with a broad range of wavelength and lifetimes (ns and ms for FL and DF (400–500 nm), respectively; tens of ms for PP (500–650 nm)). DF of the chromophore originates from triplet–triplet annihilation, which has been well reported in the literature.[59–61]

Thermoresponse of multiple luminescence

PL of the chromophore is highly sensitive to temperature. With lowering temperature, both fluorescence and phosphorescence emissions are enhanced. However, the value of I_{525}/I_{405} (I_{525} and I_{405} are the intensity of phosphorescence at 525 nm and fluorescence at 405 nm, respectively) increases with lowering temperature (Fig. S6, ESI†), demonstrating that phosphorescence is more sensitive to temperature than fluorescence. The emission of the chromophore films enhances and changes from deep blue to blue-white with decreasing temperature. CIE chromaticity coordinates shift linearly with lowering temperature (Fig. 2d). Such change in brightness and colour at various temperatures enables visual temperature sensing. On the other hand, phosphorescence fading of the crystal films becomes much slower at lower temperatures, which can be readily observed by the naked eye, and captured using a commercial mobile phone camera. The phosphorescence lifetime (at 525 nm) increases linearly from 110 to 420 ms on lowering the temperature from 273 to 203 K (Fig. 2e), following a linear relationship $Y = -4.675X + 1371$ ($R = 0.9926$). Such a linear relationship of long phosphorescence lifetime against temperature is valuable for further quantitative temperature sensing. The colour evolution of the crystal films is also temperature-dependent. Colour evolution of the crystal films is obvious and can be readily captured by a commercial mobile phone camera at low temperatures (*e.g.* 203 K). For instance, the crystal film emits blue-white light at 203 K under a UV lamp. The emission colour changes to white and green in turn, and fades gradually after switching off the UV lamp, which is

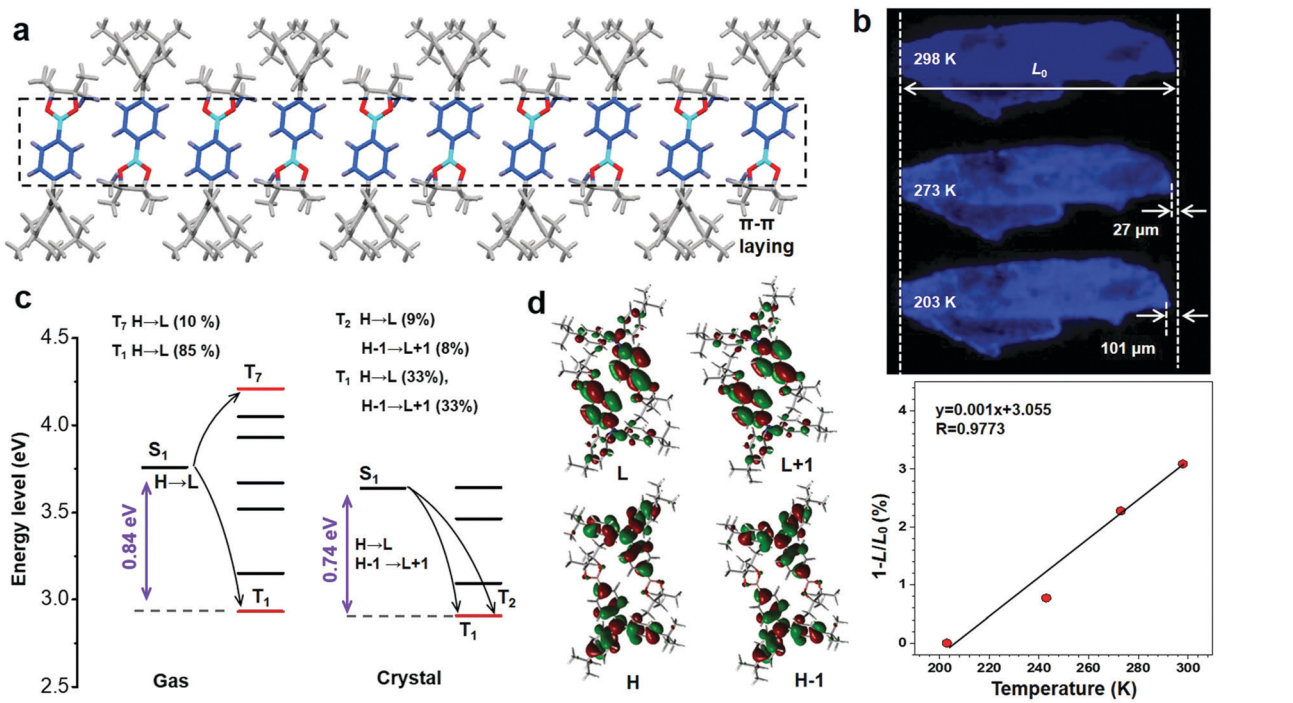

Fig. 3 (a) Packing of TBBU molecules with side-by-side intermolecular phenyl and borate rings laying nearly on a coplane (π–π laying). (b) Fluorescence microscopy images of the crystals at various temperatures. (c) The TD-DFT calculated singlet (S_1) and triplet (T_n) states for the chromophore in the gas and crystalline phases at the B3LYP/6-31G* level. (d) Involved frontier molecular orbitals of the HOMO and LUMO for the chromophore in crystals.

different from that at 298 K (Fig. 2d). Such thermoresponsive colour evolution offers an extra signal channel for further visual temperature sensing. To understand the thermoresponsive luminescence, time-resolved photoluminescence (TRPL) spectra of FL and DF of the crystal film at various temperatures were also collected. The lifetimes of both FL and DF increase slightly with lowering temperature (Fig. S7–S10 and Tables S1–S4, ESI†). For example, the lifetime of the DF at 405 nm increases from 5.5 to 7.6 ms (Fig. 2f), while the lifetime of the fluorescence at 405 nm rises slightly from 1.3 to 1.5 ns, with lowering the temperature from 273 to 203 K. Consequently, the remarkable thermoresponsive persistent phosphorescence (TPP) at a wavelength of 500–650 nm, together with DF and fluorescence at a wavelength of 400–500 nm with well-separated lifetimes (hundreds of ms, ms, and ns, respectively), gives rise to multiple visual signals including colour, colour evolution, brightness, and fading rates, for quantitative temperature sensing.

Crystal powders of the chromophore do not undergo any thermal transitions in the temperature range investigated (*i.e.* 298–203 K, Fig. S11, ESI†).[54] Therefore, the TPP of the chromophore is not related to thermal transitions, different from the organic TRP compounds reported (Fig. S1, ESI†). To understand the TPP mechanism, single crystals of the chromophore were analysed. The chromophore molecules are aligned in a head-to-tail manner thanks to their asymmetric D–π–A skeleton. Side-by-side packed intermolecular phenyl and borate rings laying nearly in a co-plane dominate with abundant intermolecular interactions including C–H···O, π–H···O, and C–H···π (Fig. 3a and Fig. S12, ESI†). The extraordinary head-to-tail alignment with side-by-side packed intermolecular phenyl and borate rings of the chromophore facilitates the geometric contact of the neighbouring molecules and their interaction. The multiple interactions between adjacent molecules stabilize the excited excitons and promote consequently phosphorescence. With raising temperature, the crystals expand, which weakens the intermolecular interactions. Consequently, molecular motion is activated, which consumes the energy of excited states and leads to a faint phosphorescence. Thermal expansion of the chromophore crystals was *in situ* monitored using a fluorescence microscope (Fig. 3b). The length of the crystals is noticeably increased with raising temperature from 203 to 298 K.

Time-dependent density functional theory (TD-DFT) calculations were performed for the chromophore in the gas and crystalline phases to gain deep insight into its TPP. The energy gap between the lowest excited singlet state (S_1) and the lowest excited triplet state (T_1), ΔE_{ST}, is 0.84 eV with 2 intersystem crossing (ISC) channels for isolated chromophore molecules in the gas phase. ΔE_{ST} of the chromophore dimers in crystals decreases to 0.74 eV with 4 ISC channels (Fig. 3c, Fig. S13 and S14, ESI†). The lower ΔE_{ST} and more ISC channels of the chromophore dimers reveal that the interaction between neighbouring molecules is favourable for their persistent phosphorescence. With lowering temperature, molecular motion of the chromophore is alleviated, accompanied by enhanced interaction between neighbouring

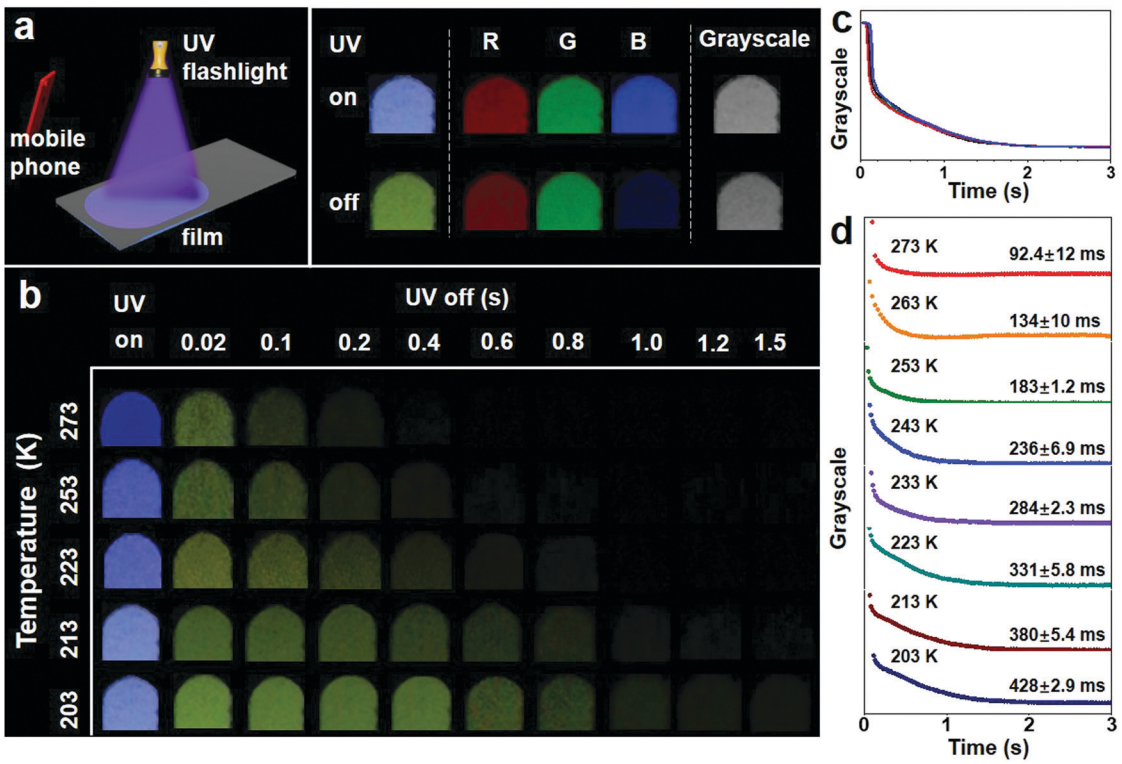

Fig. 4 (a) Illustration of temperature sensing using the crystal films. (b) Digital images of the crystal films at various temperatures. (c) Plots of grayscale (*G*) value against time for the crystal films (at 203 K). (d) Representative plots of grayscale (*G*) value against time at various temperatures and the associated fitting curve. Five parallel measurements were carried out for each temperature.

molecules, leading to boosted phosphorescence emission. The rate constant of nonradiative decay (k_{nr}) from T_1 to S_0 was calculated. The crystals have a large k_{nr} value of 7.249 s^{-1} at 273 K (Tables S5–S7, ESI†), which decreases drastically by an order of magnitude (0.697 s^{-1}) at a low temperature (*i.e.* 203 K). Meanwhile, with lowering the temperature from 273 to 203 K, the quantum yield of phosphorescence increases from 2.0 to 16%.

Temperature sensors based on crystal films

Encouraged by the linear relationship of the long phosphorescence lifetime with temperature, we further constructed temperature sensors based on crystal films of the chromophore. A method through phosphorescence lifetime and image analysis (PLIA) of the crystal films was used for visual and quantitative temperature sensing. The crystal films were subjected to various temperatures and excited with a UV lamp at 365 nm. Videos were recorded using a commercial mobile phone camera (Fig. 4a). Images at various times were extracted from the videos (Fig. 4b). The red, green, and blue (RGB) values of the images were calculated. The grayscale (G) of the images was determined based on the RGB values.[42,62,63] The plots of the G value against time at various temperatures were obtained (Fig. 4c). The G value drops exponentially as a function of time. The phosphorescence lifetimes at various temperatures were further obtained by data fitting (Fig. 4d). To check reproducibility, five parallel measurements were carried out for each temperature. The phosphorescence lifetimes of the crystal films at various temperatures by PLIA are close to those determined by time-resolved photoluminescence spectra (TRPL) (Fig. 2e and Table S8, ESI†), following $Y = -4.509X + 1333$ ($R = 0.9944$).

Polymer films doped with the chromophore

The chromophore was further used to dope polymers. A couple of commercial polymers including poly(ethylene oxide)/poly(propylene oxide) triblock copolymer (EPE, Pluronic F-127), polystyrene (PS), poly(methyl methacrylate) (PMMA) and fluororubber (FKM) were utilized as polymer matrices due to its good film processability and eco-friendliness. Among the polymers, the doped EPE films (containing 10 wt% chromophore) exhibit the most intensive and obvious phosphorescence at low temperatures (*e.g.* 233 K). The optimized EPE films doped with 10 wt% chromophore with a thickness of 0.42 mm show bright fluorescence and obvious phosphorescence at low temperatures (*e.g.* 233 K) (Fig. S15, S16 and Table S9, ESI†). XRD spectra of the polymer films demonstrate that the chromophore forms crystals in the doped polymer films (Fig. S17, ESI†). Fluorescence microscopy images show that microcrystals of the chromophore with a size of approximately 100 μm are uniformly dispersed in the polymer matrix (Fig. S18, ESI†). The polymer films emit intense blue light under UV lamp (365 nm). The colour of the polymer films turns into white and green in turn, and fades gradually, after removing UV radiation. Delayed PL of the polymer films show double emission peaked at 405 and 525 nm (Fig. S19, ESI†). With increasing decay time, the PL intensity at 405 nm drops drastically with respect to the peak at 525 nm. CIE chromaticity coordinates shift linearly from (0.17, 0.11) to (0.38, 0.60), passing through the white region (0.28, 0.38). Such colour evolution of the polymer films resembles that of crystal films.

Phosphorescence of the doped polymer film is also sensitive to temperature (Fig. S20 and S21, ESI†). With lowering temperature, the emission colour of the doped film changes from deep blue to blue-white, which is similar to that of the chromophore crystals (Fig. 2). Moreover, colour evolution of the polymer films is also temperature-dependent (Fig. S22, ESI†). With lowering temperature, colour evolution of the polymer films is more observable. For instance, at 203 K, polymer films emit bright blue-white light under UV radiation (365 nm). The colour changes into white, green, and fades gradually after switching off the UV lamp. CIE chromaticity coordinates shift

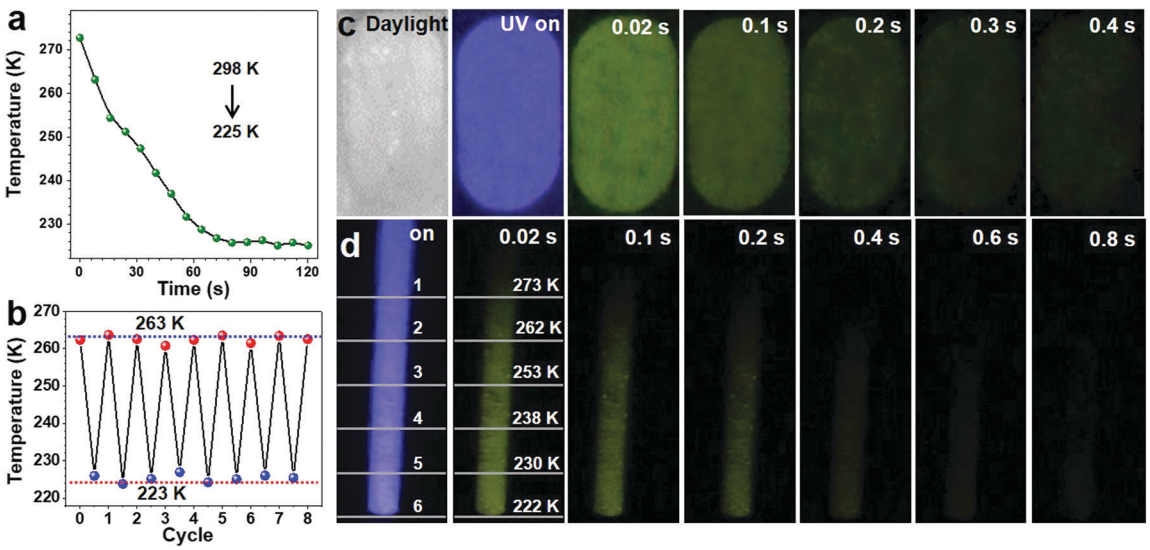

Fig. 5 Temperature sensing using the doped polymer films. (a) Quick response of the polymer films to temperature variation (from 298 to 225 K). (b) Repeatability of temperature sensing. (c) Sensing the temperature of a piece of ice and (d) sensing the temperature gradient.

linearly from (0.20, 0.19) to (0.40, 0.57), passing through the white region (0.26, 0.31) again, with a delay from 1 to 100 ms. Meanwhile, the phosphorescence lifetime increases linearly from 40 to 340 ms with lowering the temperature from 273 to 203 K (Fig. 2e and Fig. S23, ESI†), following $Y = -4.468X + 1244$ ($R = 0.9922$). Variation in the lifetime of the polymer films by 8-fold is more obvious than that of the crystal films (4-fold), which favours further quantitative temperature sensing. Moreover, the phosphorescence lifetime of the doped polymer films is lower systematically than that of crystal films, likely due to the less perfect crystalline structure of the chromophore in the doped polymer films (Fig. S18 and S19, ESI†).

The PLIA method was also applied to the doped polymer films (Fig. S24 and S25, ESI†). The lifetimes determined by PLIA are close to those by TRPL again (Fig. 2e and Table S10, ESI†), following $Y = -4.421X + 1232$ ($R = 0.9902$). Moreover, the response of the doped polymer films to temperature variation was further tested. The doped film was subjected to a low temperature (*e.g.* 225 K). The temperature value determined by PLIA stabilizes within 75 s (Fig. 5a). The reproducibility of the polymer films for temperature sensing was also evaluated (Fig. 5b). The doped polymer films were subjected to the temperature being repeatedly switched between 263 and 223 K. Temperature sensing is repeatable over 8 cycles. Such rapid response and good reproducibility of the doped polymer films to temperature variation are crucial to practical temperature sensing.

Temperature sensing with the doped polymer films

Encouraged by the good reliability and accuracy, as well as quick response, the PLIA method was used to test the temperature of ice. The polymer films emit blue-white light upon UV radiation (Fig. 5c). Compared with the images at various temperatures (Fig. S24, ESI†), the temperature of the ice is estimated in the range of 233–253 K. The colour changes into white rapidly, then green, and fades gradually after switching off the UV lamp. By applying PLIA, the lifetime is calculated to be 165 ± 2.8 ms (Fig. S26 and Table S11, ESI†). Temperature is determined to be 241.0 ± 0.4 K, close to that by a thermometer (241.5 K, Fig. S27, ESI†). The polymer films were further used to sense temperature gradient (Fig. 5d and Fig. S28, ESI†). The emission colour changes from blue-white to deep blue from bottom to top, indicating a temperature gradient from 213 to 273 K, by comparing the images at various temperatures (Fig. S24, ESI†). After switching off the UV lamp, the colour changes into white quickly, and green, and then fades gradually from top to bottom. The temperatures of six regions are determined to be 273, 262, 253, 238, 230, and 222 K from top to bottom (Table S12, ESI†), respectively, which are in the temperature range designed (298–213 K from top to bottom).

Taking full advantage of the thermoresponsive multiple luminescence, especially remarkable TPP of the chromophore, the PLIA based on the doped polymer films possesses overwhelming merits contrasting to conventional materials. Firstly, multiple visual signals including brightness, colour, colour evolution, and fading rates are available for temperature sensing. Secondly, this method allows quick and quantitative determination of temperature with good reliability and accuracy. In particular, the linear relationship of long lifetime against temperature is desirable for practical temperature sensing. Thirdly, the lifetime of PP is independent of the shape and size of the samples, the distance between the samples and detectors, and excitation. Thus, this method eliminates the need for complicated calibration procedures.

Conclusions

In summary, we report unusual full-type photoluminescence including simultaneous fluorescence (FL), delayed fluorescence (DF), and persistent phosphorescence (PP) from an organic single-component chromophore. Unique aggregation-induced phosphorescence (AIP) and obvious thermoresponsive persistent phosphorescence (TPP) are systematically investigated. Emission of the chromophore crystals turns from blue to white and green in turn, and fades finally after switching off the UV lamps. The colour evolution of the chromophore is related to its multiple luminescence with a broad range of wavelengths and lifetimes (ns and ms for FL and DF (400–500 nm), respectively; tens of ms for PP (500–650 nm)). Moreover, TPP, coupled with thermoresponsive FL and DF of the chromophore, results in abundant signals such as emission brightness, colour, colour evolution, and fading rates for visual temperature sensing. More interestingly, polymer films doped with the chromophore show amplified TPP characteristics. The phosphorescence lifetime of the doped film is linearly prolonged by 8-fold with lowering the temperature. Finally, phosphorescence lifetime and image analysis (PLIA) is carried out for rapid, visual, and quantitative temperature sensing. Given the good reliability and accuracy, easy operation, and simple devices, the PLIA based on this chromophore provides an ideal platform for facile temperature sensing.

Author contributions

J. Ma and Y. Zhou contributed equally to performing the experiments. G. Liang designed the project and wrote the paper. All authors contributed to the general discussion.

Conflicts of interest

There are no conflicts to declare.

Acknowledgements

The financial support was partially from NSFC (21374136), and the Fundamental Research Funds for the Central Universities (17lgjc03 and 18lgpy04).

Notes and references

1 K. C. Xie, X. S. Li and T. Cao, Theory and Ab Initio Calculation of Optically Excited States-Recent Advances in 2D Materials, *Adv. Mater.*, 2019, 1904306.

2 D. F. Li, J. Wang and X. Ma, White-Light-Emitting Materials Constructed from Supramolecular Approaches, *Adv. Opt. Mater.*, 2018, **6**, 1800273.
3 K. Kokado and K. Sada, Consideration of Molecular Structure in the Excited State to Design New Luminogens with Aggregation-Induced Emission, *Angew. Chem., Int. Ed.*, 2019, **58**, 8632–8639.
4 X. Kang and M. Z. Zhu, Tailoring the Photoluminescence of Atomically Precise Nanoclusters, *Chem. Soc. Rev.*, 2019, **48**, 2422–2457.
5 W. J. Jie, Z. B. Yang, G. X. Bai and J. H. Hao, Luminescence in 2D Materials and van der Waals Heterostructures, *Adv. Opt. Mater.*, 2018, **6**, 1701296.
6 Y. Lei, W. Dai, J. Guan, S. Guo, F. Ren, Y. Zhou, J. Shi, B. Tong, Z. Cai, J. Zheng and Y. Dong, Wide-Range Color-Tunable Ultralong Organic Phosphorescence Materials for Printable and Writable Security Inks, *Angew. Chem., Int. Ed.*, 2020, **59**, 16054–16060.
7 Y. Wang, J. Yang, Y. Tian, M. Fang, Q. Liao, L. Wang, W. Hu, B. Z. Tang and Z. Li, Persistent Organic Room Temperature Phosphorescence: What Is the Role of Molecular Dimers?, *Chem. Sci.*, 2020, **11**, 833–838.
8 S. Wang, M. Xu, K. Huang, J. Zhi, C. Sun, K. Wang, Q. Zhou, L. Gao, Q. Jia, H. Shi, Z. An, P. Li and W. Huang, Biocompatible Metal-Free Organic Phosphorescent Nanoparticles for Efficiently Multidrug-Resistant Bacteria Eradication, *Sci. China Mater.*, 2020, **63**, 316–324.
9 Y. Ren, Z. Yang, Y. Wang, M. Li, J. Qiu, Z. Song, J. Yu, A. Ullah and I. Khan, Reversible Multiplexing for Optical Information Recording, Erasing, and Reading-out in Photochromic $BaMgSiO_4$:Bi^{3+} Luminescence Ceramics, *Sci. China Mater.*, 2020, **63**, 582–592.
10 Z. Yang, E. Ubba, Q. Huang, Z. Mao, W. Li, J. Chen, J. Zhao, Y. Zhang and Z. Chi, Enabling Dynamic Ultralong Organic Phosphorescence in Molecular Crystals Through the Synergy Between Intramolecular and Intermolecular Interactions, *J. Mater. Chem. C*, 2020, **8**, 7384–7392.
11 X. Yang, Q. Wang, P. Hu, C. Xu, W. Guo, Z. Wang, Z. Mao, Z. Yang, C. Liu, G. Shi, L. Chen, B. Xu and Z. Chi, Achieving Remarkable and Reversible Mechanochromism from a Bright Ionic AIEgen with High Specificity for Mitochondrial Imaging and Secondary Aggregation Emission Enhancement for Long-Term Tracking of Tumors, *Mater. Chem. Front.*, 2020, **4**, 941–949.
12 Q. Miao, C. Xie, X. Zhen, Y. Lyu, H. Duan, X. Liu, J. V. Jokerst and K. Pu, Molecular Afterglow Imaging with Bright, Biodegradable Polymer Nanoparticles, *Nat. Biotechnol.*, 2017, **35**, 1102–1110.
13 Y. Jiang, J. Huang, X. Zhen, Z. Zeng, J. Li, C. Xie, Q. Miao, J. Chen, P. Chen and K. Pu, A Generic Approach Towards Afterglow Luminescent Nanoparticles for Ultrasensitive in Vivo Imaging, *Nat. Commun.*, 2019, **10**, 2064.
14 L. Xiao, Y. S. Wu, Z. Y. Yu, Z. Z. Xu, J. B. Li, Y. P. Liu, J. N. Yao and H. B. Fu, Room-Temperature Phosphorescence in Pure Organic Materials: Halogen Bonding Switching Effects, *Chem. – Eur. J.*, 2018, **24**, 1801–1805.
15 L. Xiao, Y. S. Wu, J. W. Chen, Z. Y. Yu, Y. P. Liu, J. N. Yao and H. B. Fu, Highly Efficient Room-Temperature Phosphorescence from Halogen-Bonding-Assisted Doped Organic Crystals, *J. Phys. Chem. A*, 2017, **121**, 8652–8658.
16 T. Wang, C. Zhou, X. Y. Zhang and D. Xu, Waterborne Polyurethanes Prepared from Benzophenone Derivatives with Delayed Fluorescence and Room-Temperature Phosphorescence, *Polym. Chem.*, 2018, **9**, 1303–1308.
17 S. Y. Tao, S. Y. Lu, Y. J. Geng, S. J. Zhu, S. A. T. Redfern, Y. B. Song, T. L. Feng, W. Q. Xu and B. Yang, Design of Metal-Free Polymer Carbon Dots: A New Class of Room-Temperature Phosphorescent Materials, *Angew. Chem., Int. Ed.*, 2018, **57**, 2393–2398.
18 T. D. Liu, G. Q. Zhang, R. E. Evans, C. O. Trindle, Z. Altun, C. A. DeRosa, F. Wang, M. Zhuang and C. L. Fraser, Phosphorescence Tuning Through Heavy Atom Placement in Unsymmetrical Difluoroboron Beta-Diketonate Materials, *Chem. – Eur. J.*, 2018, **24**, 1859–1869.
19 Y. Su, S. Z. F. Phua, Y. Li, Y. Zhou, D. Jana, G. Liu, W. Lim, W. Ong, C. Yang and Y. Zhao, Ultralong Room Temperature Phosphorescence from Amorphous Organic Materials Toward Confidential Information Encryption and Decryption, *Sci. Adv.*, 2018, **4**, 9732.
20 W. B. Liang, C. C. Fan, Y. Zhuo, Y. N. Zheng, C. Y. Xiong, Y. Q. Chai and R. Yuan, Multiparameter Analysis-Based Electrochemi Luminescent Assay for Simultaneous Detection of Multiple Biomarker Proteins on a Single Interface, *Anal. Chem.*, 2016, **88**, 4940–4948.
21 Y. Shoji, Y. Ikabata, Q. Wang, D. Nemoto, A. Sakamoto, N. Tanaka, J. Seino, H. Nakai and T. Fukushima, Unveiling a New Aspect of Simple Arylboronic Esters: Long-Lived Room-Temperature Phosphorescence from Heavy-Atom-Free Molecules, *J. Am. Chem. Soc.*, 2017, **139**, 2728–2733.
22 K. Kanosue and S. Ando, Polyimides with Heavy Halogens Exhibiting Room-Temperature Phosphorescence with Very Large Stokes Shifts, *ACS Macro Lett.*, 2016, **5**, 1301–1305.
23 G. Q. Zhang, G. M. Palmer, M. Dewhirst and C. L. Fraser, A Dual-Emissive-Materials Design Concept Enables Tumour Hypoxia Imaging, *Nat. Mater.*, 2009, **8**, 747–751.
24 G. Q. Zhang, J. W. Lu, M. Sabat and C. L. Fraser, Polymorphism and Reversible Mechanochromic Luminescence for Solid-State Difluoroboron Avobenzone, *J. Am. Chem. Soc.*, 2010, **132**, 2160–2162.
25 G. Zhang, J. Chen, S. J. Payne, S. E. Kooi, J. N. Demas and C. L. Fraser, Multi-Emissive Difluoroboron Dibenzoylmethane Polylactide Exhibiting Intense Fluorescence and Oxygen-Sensitive Room-Temperature Phosphorescence, *J. Am. Chem. Soc.*, 2007, **129**, 8942–8943.
26 C. A. DeRosa, J. Samonina-Kosicka, Z. Y. Fan, H. C. Hendargo, D. H. Weitzel, G. M. Palmer and C. L. Fraser, Oxygen Sensing Difluoroboron Dinaphthoylmethane Polylactide, *Macromolecules*, 2015, **48**, 2967–2977.
27 X. P. Zhang, T. Q. Xie, M. X. Cui, L. Yang, X. X. Sun, J. Jiang and G. Q. Zhang, General Design Strategy for Aromatic Ketone-Based Single-Component Dual-Emissive Materials, *ACS Appl. Mater. Interfaces*, 2014, **6**, 2279–2284.

28 X. F. Wu, H. Hang, H. Li, Y. H. Chen, H. Tong and L. X. Wang, Water-Dispersible Hyperbranched Conjugated Polymer Nanoparticles with Sulfonate Terminal Groups for Amplified Fluorescence Sensing of Trace TNT in Aqueous Solution, *Mater. Chem. Front.*, 2017, **1**, 1875–1880.

29 H. Hao, C. Xu, H. Luo, J. Yang, C. Liu, B. Xu, G. Shi, X. Xing and Z. Chi, An AIE Luminogen-Based Electropolymerized Film: An Ultrasensitive Fluorescent Probe for TNP and Fe^{3+} in Water, *Mater. Chem. Front.*, 2021, **5**, 492–499.

30 W. J. Zhao, Z. K. He, J. W. Y. Lam, Q. Peng, H. L. Ma, Z. G. Shuai, G. X. Bai, J. H. Hao and B. Z. Tang, Rational Molecular Design for Achieving Persistent and Efficient Pure Organic Room-Temperature Phosphorescence, *Chem*, 2016, **1**, 592–602.

31 J. Yang, X. Zhen, B. Wang, X. M. Gao, Z. C. Ren, J. Q. Wang, Y. J. Xie, J. R. Li, Q. Peng, K. Y. Pu and Z. Li, The Influence of the Molecular Packing on the Room Temperature Phosphorescence of Purely Organic Luminogens, *Nat. Commun.*, 2018, **9**, 840.

32 Y. J. Xie, Y. W. Ge, Q. Peng, C. G. Li, Q. Q. Li and Z. Li, How the Molecular Packing Affects the Room Temperature Phosphorescence in Pure Organic Compounds: Ingenious Molecular Design, Detailed Crystal Analysis, and Rational Theoretical Calculations, *Adv. Mater.*, 2017, **29**, 1606829.

33 Z. Yang, C. Xu, W. Li, Z. Mao, X. Ge, Q. Huang, H. Deng, J. Zhao, F. L. Gu, Y. Zhang and Z. Chi, Boosting the Quantum Efficiency of Ultralong Organic Phosphorescence up to 52% via Intramolecular Halogen Bonding, *Angew. Chem., Int. Ed.*, 2020, **59**, 17451–17455.

34 M. Chen, H. Nie, B. Song, L. Li, J. Z. Sun, A. Qin and B. Z. Tang, Triphenylamine-Functionalized Tetraphenylpyrazine: Facile Preparation and Multifaceted Functionalities, *J. Mater. Chem. C*, 2016, **4**, 2901–2908.

35 X. Zhen, Y. Tao, Z. F. An, P. Chen, C. J. Xu, R. F. Chen, W. Huang and K. Y. Pu, Ultralong Phosphorescence of Water-Soluble Organic Nanoparticles for In Vivo Afterglow Imaging, *Adv. Mater.*, 2017, **29**, 1606665.

36 S. Z. Cai, H. F. Shi, D. Tian, H. L. Ma, Z. C. Cheng, Q. Wu, M. X. Gu, L. Huang, Z. F. An, Q. Peng and W. Huang, Enhancing Ultralong Organic Phosphorescence by Effective pi-Type Halogen Bonding, *Adv. Funct. Mater.*, 2018, **28**, 1705045.

37 J. B. Wei, B. Y. Liang, R. H. Duan, Z. Cheng, C. L. Li, T. L. Zhou, Y. P. Yi and Y. Wang, Induction of Strong Long-Lived Room-Temperature Phosphorescence of N-Phenyl-2-naphthylamine Molecules by Confinement in a Crystalline Dibromobiphenyl Matrix, *Angew. Chem., Int. Ed.*, 2016, **55**, 15589–15593.

38 B. Zhou and D. P. Yan, Simultaneous Long-Persistent Blue Luminescence and High Quantum Yield Within 2D Organic-Metal Halide Perovskite Micro/Nanosheets, *Angew. Chem., Int. Ed.*, 2019, **58**, 15128–15135.

39 S. Tian, H. Ma, X. Wang, A. Lv, H. Shi, Y. Geng, J. Li, F. Liang, Z.-M. Su, Z. An and W. Huang, Utilizing d–pπ Bonds for Ultralong Organic Phosphorescence, *Angew. Chem., Int. Ed.*, 2019, **58**, 6645–6649.

40 A. Seeboth, D. Lotzsch, R. Ruhmann and O. Muehling, Thermochromic Polymers-Function by Design, *Chem. Rev.*, 2014, **114**, 3037–3068.

41 K. Totani, Y. Okada, S. Hirata, M. Vacha and T. Watanabe, Thermoresponsive Persistent Phosphorescent Color Change Using Efficient Thermally Activated Reverse Energy Transfer with a Large Energy Difference, *Adv. Opt. Mater.*, 2013, **1**, 283–288.

42 W. Qin, J. Ma, Y. Zhou, Q. Hu, Y. Zhou and G. Liang, Simultaneous Promotion of Efficiency and Lifetime of Organic Phosphorescence for Self-Referenced Temperature Sensing, *Chem. Eng. J.*, 2020, **400**, 125934.

43 X. Zhen, C. Xie and K. Pu, Temperature-Correlated Afterglow of a Semiconducting Polymer Nanococktail for Imaging-Guided Photothermal Therapy, *Angew. Chem., Int. Ed.*, 2018, **57**, 3938–3942.

44 T. Takeda, S. Yamamoto, M. Mitsuishi and T. Akutagawa, Thermoresponsive Amphipathic Fluorescent Organic Liquid, *J. Phys. Chem. C*, 2018, **122**, 9593–9598.

45 X. L. Luo, J. N. Li, C. H. Li, L. P. Heng, Y. Q. Dong, Z. P. Liu, Z. S. Bo and B. Z. Tang, Reversible Switching of the Emission of Diphenyldibenzofulvenes by Thermal and Mechanical Stimuli, *Adv. Mater.*, 2011, **23**, 3261–3265.

46 Y. Sagara, K. Kubo, T. Nakamura, N. Tamaoki and C. Weder, Temperature-Dependent Mechanochromic Behavior of Mechanoresponsive Luminescent Compounds, *Chem. Mater.*, 2017, **29**, 1273–1278.

47 H. C. Zhu, S. Y. Weng, H. Zhang, H. Z. Yu, L. Kong, Y. L. Zhong, Y. P. Tian and J. X. Yang, A Novel Carbazole Derivative Containing Fluorobenzene Unit: Aggregation-Induced Fluorescence Emission, Polymorphism, Mechanochromism and Non-Reversible Thermo-Stimulus Fluorescence, *CrystEngComm*, 2018, **20**, 2772–2779.

48 H. Wang, Y. Q. Wu, P. Tao, X. Fan and G. C. Kuang, BODIPY-Based Oligo(ethylene glycol) Dendrons as Fluorescence Thermometers: When Thermoresponsiveness Meets Intramolecular Electron/Charge Transfer, *Chem. – Eur. J.*, 2014, **20**, 16634–16643.

49 C. H. Li, Y. X. Zhang, J. M. Hu, J. J. Cheng and S. Y. Liu, Reversible Three-State Switching of Multicolor Fluorescence Emission by Multiple Stimuli Modulated FRET Processes Within Thermoresponsive Polymeric Micelles, *Angew. Chem., Int. Ed.*, 2010, **49**, 5120–5124.

50 G. Liang, J. Wu, H. Gao, Q. Wu, J. Lu, F. Zhu and B. Z. Tang, General Platform for Remarkably Thermoresponsive Fluorescent Polymers with Memory Function, *ACS Macro Lett.*, 2016, **5**, 909–914.

51 G. Liang, F. Ren, H. Gao, Q. Wu, F. Zhu and B. Z. Tang, Continuously-Tunable Fluorescent Polypeptides Through a Polymer-Assisted Assembly Strategy, *Polym. Chem.*, 2016, **7**, 5181–5187.

52 B. Zhou, Q. Zhao, L. Tang and D. Yan, Tunable Room Temperature Phosphorescence and Energy Transfer in Ratiometric Co-Crystals, *Chem. Commun.*, 2020, **56**, 7698–7701.

53 Q. Wang, X. Y. Dou, X. H. Chen, Z. H. Zhao, S. Wang, Y. Z. Wang, K. Y. Sui, Y. Q. Tan, Y. Y. Gong, Y. M. Zhang and

W. Z. Yuan, Reevaluating Protein Photoluminescence: Remarkable Visible Luminescence upon Concentration and Insight into the Emission Mechanism, *Angew. Chem., Int. Ed.*, 2019, **58**, 12667–12673.

54 Y. Zhou, W. Qin, C. Du, H. Gao, F. Zhu and G. Liang, Long-Lived Room-Temperature Phosphorescence for Visual and Quantitative Detection of Oxygen, *Angew. Chem., Int. Ed.*, 2019, **58**, 12102–12106.

55 J. Mei, N. L. C. Leung, R. T. K. Kwok, J. W. Y. Lam and B. Z. Tang, Aggregation-Induced Emission: Together We Shine, United We Soar!, *Chem. Rev.*, 2015, **115**, 11718–11940.

56 J. Mei, Y. N. Hong, J. W. Y. Lam, A. J. Qin, Y. H. Tang and B. Z. Tang, Aggregation-Induced Emission: The Whole Is More Brilliant than the Parts, *Adv. Mater.*, 2014, **26**, 5429–5479.

57 Y. C. Chen, J. W. Y. Lam, R. T. K. Kwok, B. Liu and B. Z. Tang, Aggregation-Induced Emission: Fundamental Understanding and Future Developments, *Mater. Horiz.*, 2019, **6**, 428–433.

58 T. Wang, X. G. Su, X. P. Zhang, X. C. Nie, L. K. Huang, X. Y. Zhang, X. Sun, Y. Luo and G. Q. Zhang, Aggregation-Induced Dual-Phosphorescence from Organic Molecules for Nondoped Light-Emitting Diodes, *Adv. Mater.*, 2019, **31**, 1904273.

59 N. Yanai and N. Kimizuka, Stimuli-Responsive Molecular Photon Upconversion, *Angew. Chem., Int. Ed.*, 2020, **59**, 10252–10264.

60 Y. W. Xu, X. M. Liang, X. H. Zhou, P. S. Yuan, J. D. Zhou, C. Wang, B. B. Li, D. H. Hu, X. F. Qiao, X. F. Jiang, L. L. Liu, S. J. Su, D. G. Ma and Y. G. Ma, Highly Efficient Blue Fluorescent OLEDs Based on Upper Level Triplet-Singlet Intersystem Crossing, *Adv. Mater.*, 2019, **31**, 1803788.

61 M. H. C. van Son, A. M. Berghuis, F. Eisenreich, B. de Waal, G. Vantomme, J. G. Rivas and E. W. Meijer, Highly Ordered 2D-Assemblies of Phase-Segregated Block Molecules for Upconverted Linearly Polarized Emission, *Adv. Mater.*, 2020, **32**, 2004775.

62 Z. J. Qiu, W. J. Zhao, M. K. Cao, Y. Q. Wang, J. W. Y. Lam, Z. Zhang, X. Chen and B. Z. Tang, Dynamic Visualization of Stress/Strain Distribution and Fatigue Crack Propagation by an Organic Mechanoresponsive AIE Luminogen, *Adv. Mater.*, 2018, **30**, 1803924.

63 Z. J. Qiu, E. K. K. Chu, M. J. Jiang, C. Gui, N. Xie, W. Qin, P. Alam, R. T. K. Kwok, J. W. Y. Lam and B. Z. Tang, A Simple and Sensitive Method for an Important Physical Parameter: Reliable Measurement of Glass Transition Temperature by AIEgens, *Macromolecules*, 2017, **50**, 7620–7627.

